2013

A feasibility study of a computer-based wind turbine blades surface flaws inspection method

Huiyi Zhang
Iowa State University

A feasibility study of a computer-based wind turbine blades surface flaws inspection method

by

Huiyi Zhang

A thesis submitted to the graduate faculty

in partial fulfillment of the requirements for the degree of

MASTER OF SCIENCE

Major: Industrial Engineering

Program of Study Committee:
John Jackman, Major Professor
Frank Peters
Vinay Dayal

Iowa State University

Ames, Iowa

2013

TABLE OF CONTENTS

Page

LIST OF FIGURES

LIST OF TABLES

ACKNOWLEDGEMENTS

I would like to thank my major professor, Dr. John Jackman, for all of his support and masterful editing assistance, and my committee members, Dr. Frank Peters and Dr. Vinay Dayal with Dr. Matt Frank for bringing me to the Wind Energy Manufacturing Laboratory (WEML).

In addition, I would like to thank the Principal Investigator, Dr. James, McCalley and the Director of Graduate Education, Dr. John Jackman for offering me the Integrative Graduate Education and Research Traineeship (IGERT) award in Wind Energy Science, Engineering, and Policy.

Finally, I would also like to thank my husband, Nathan Jackson, for bringing me to the United States and strongly encouraging me to pursue higher education. I want to also offer my appreciation to both my parents and parents-in-laws for their hours of patience, respect and love.

ABSTRACT

Visual inspection is widely used to improve the reliability of in-service products such as wind turbine blades (WTBs), aircraft surfaces, and bridges. Lowering costs by reducing maintenance hours and increasing labor safety, decreasing production and service downtimes, promoting high accuracy inspections as well as making early repair are motivating factors for having reliable visual inspection techniques. In this study, a new image processing technique was investigated to assess its ability to detect surface flaws on a WTB on-tower. The method was tested by varying the parameters of the surface flaws as well as the parameters of the method. It was found that detecting and quantifying cracks as small as hair thickness with computer-based visual inspection is feasible and the orientation of a crack was not sensitive to image processing so that the inspection camera does not need to set up at a specific angle to detect cracks. It was found that uneven background illumination was not a major concern for the edge detection methods and can be reduced by using optimized threshold number and opening images techniques with the line detection method. In addition, the accuracy of quantifying a crack was improved by reducing noise with the intersection two processed images from different methods.

CHAPTER 1: INTRODUCTION

Wind energy provides more than 3% of total U.S. electricity supply and contributes more than 10% of total electricity generation in six states with two of these states being above 20% (Chen, 2012). Most of the wind farms have installed turbines in the past 10 years and the installation capacity is expected to grow continuously at more than 25% per annum to meet the Department of Energy (DOE) 20% wind energy portfolio by 2030 (NREL report, 2008). Although the design life of a wind turbine is 20 years, early failure often affects critical components and causes significant down time, causing concern for power generation companies and investors. Rotor blades are one the largest mechanical components of a wind turbine and cannot be monitored as easily as electrical parts/controllers and smaller mechanical components such as bearings. The limited monitoring ability of current Operation and Maintenance (O&M) functions for wind farms can lead to higher energy costs and pose a threat to the development of offshore wind farms, which counts for 4% of the DOE 2030 wind energy portfolio. In addition, the general public has voiced a number of concerns about the viability of wind energy. To address part of the viability and cost concerns, research on reliable and cost-effective blade monitoring systems is warranted.

Rotor blades account for roughly 18% of the total turbine cost and have significant challenge of maintenance due to the large-scale, on-tower and non-unique complex materials. The annual O&M cost of a wind farm is 0.5 – 2.5 ¢/kWh based on the capacity and the operation years and it accounts 10 - 20% of the total COE for a wind project, based on current COE figures of 3.5 – 6 cents/kWh (Sandia-Walford, 2006).

Although lack of information on cost breakdown of components of O&M, blade failure ranks in the top third of failure rates among all the critical large mechanical components. In addition, it adds a significant downtime per failure, which is 4 days on average with expensive equipment such as cranes required along with skilled technicians (Hahn, 2006). Early inspection can help prevent severe structural damage and reduce O & M costs (SGS Group, 2010). A report by SGS group points out that there is 26% additional cost to blade manufacturers to fix a blade incident but could have been corrected by an increase of 0.64% of the total turbine blades cost to the third-party inspection company.

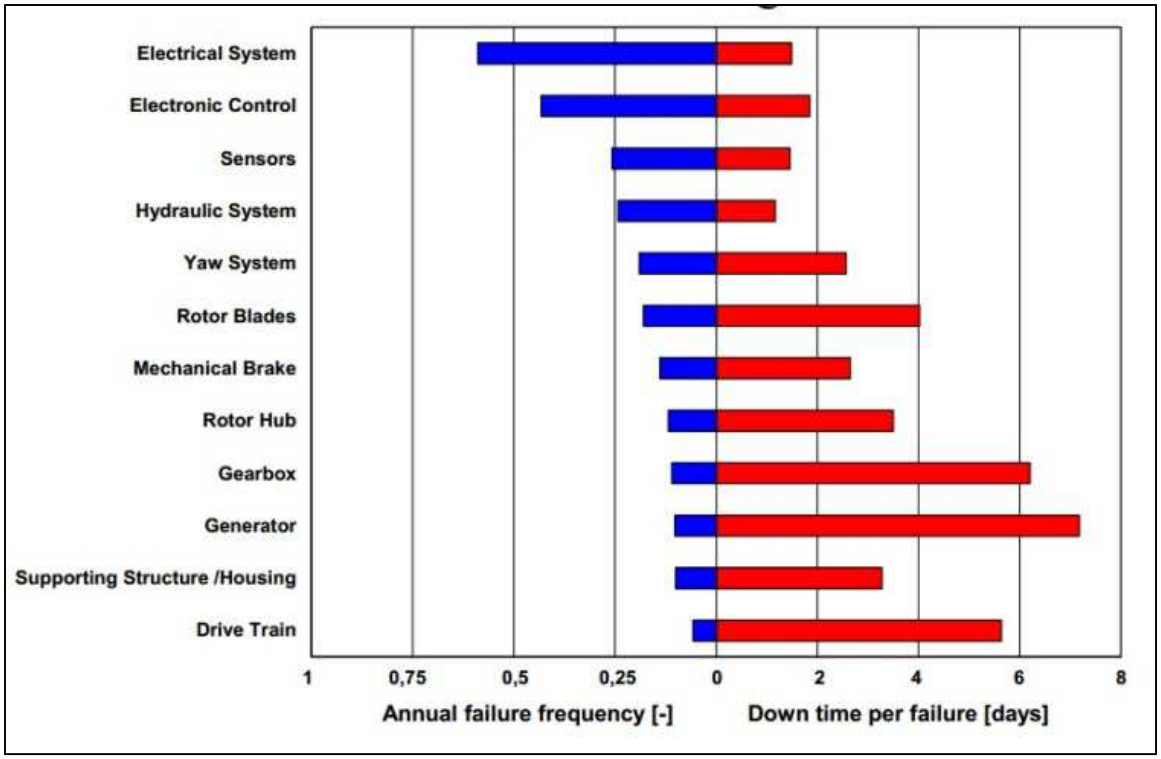

Figure 1. Failure frequency and downtime of components

WTBs Background

Turbine blades are coated with two thin layers, a gel coat layer and an environmentally friendly water-based varnish, to prevent infiltration of moisture, sand, and salt into the underlying fiberglass composite material which can lead to delamination and other types of structural damage. Depending on the stress applied to the blade surface, the thickness of gel coat may vary between 0.3mm where loads are light and 0.6mm along the leading edge where it makes first contact with wind and loads are particularly high (DNV, 2010). The health of a blade skin is a major maintenance concern and is a significant contribution to energy cost using existing on-tower inspection and repair methods. Also it is difficult to insure consistency in manual inspection because inspectors vary in their ability to detect small surface flaws that accumulate under normal blade working conditions such as hairline cracks on the blade surface. With wind energy moving offshore, the rotor blades will experience a more challenging environment – high moisture and salt – and potentially higher maintenance costs.

Blade Skin Defects

Surface damage like gel coat cracks and erosion can significantly reduce the aerodynamic efficiency of blades and lead to structural damage, which is more challenging to detect and repair. Since surface damage is relatively easy to inspect, inexpensive to repair, and will prevent future structural damage, blade surface health monitoring should be given more attention. Unfortunately, current rotor blade surface health inspection is performed by “sky workers”, technicians hanging by a rope from the tower doing close inspection and repair, or telescopes, which can be used to capture

blade surface images from the ground. Also, repair decisions are based on visual inspection which is known to cause high variability in the results. In addition, on-tower inspections add downtime to the wind turbine that will reduce annual electricity production.

This paper addresses the characteristics of the WTB surface flaws and method parameters for computer-aided visual inspection. Similar methods have been considered in aircraft health inspection. For example, a stereoscopic method has been successfully applied for a limited number of surface cracks on aircraft skins (Siegel 1997). Therefore, further investigation is warranted to assess the capability of image processing techniques in the detection of cracks in the gel coat layer. Ideally, the results of an inspection should characterize the size and severity of cracks so that the need for repair can be determined.

CHAPTER 2: RELATED RESEARCH

Wind turbine blades are not a “fit and forget” item since a variety of environmental events like lightning strikes, rain and wind erosion all cause of damage (Marsh, 2011). Wind turbine blade surface flaws can have a severe impact on fatigue experienced by the turbine blades and lead to early “wear and tear” damage. Examining early surface flaws and repairing on time can prevent future structural damages, reduce operation downtime, and save O & M costs.

More rotors in operation and rotors increasing in operation hours lead to increased blade maintenance. Until recently, wind farm operators neglected inspection and preventative maintenance. Comparing to commercial aircrafts, WTB received less than 1/8 hours of maintenance and is required to operate 8 times longer (Wood, 2011). Many blades are already past their warranty periods, especially in European countries. Current wind turbine surface health inspection methods include a group of sky workers walking on the wind turbine blades over 300ft above ground via ropes attached to their bodies. Crawlers or platform are also used to move maintenance workers along the rotor blades. Current blade inspection of SGS group takes 30 hours/turbine with inspector rates at $80/hour and UT scanner rates $220/day (SGS, 2010). Sky working is expensive and poses serious safety risks to workers. Crawlers and platforms improve the working environment of site employees and reduce the stresses and dangers associated with maintenance but still add downtime. All three methods use sky workers to perform close inspections, laminate repair, infusion, gel-coat repair, and blade cleaning. They must work with materials like polyester, vinyl ester and epoxy resins, along with glass,

carbon, aramid and bio-composite fibers. Therefore, well-trained site workers are necessary for performing the maintenance work. A new approach is to use a climbing robot with a ground-based control station to work along rotor blades and to capture images with high resolution camera (GE reports, 2012). Image processing techniques or experienced engineers then analyze the images that the robots obtained. Rosa Guido in Italy had published a paper on developing a low-cost climbing robot for offshore wind turbine blades inspection in 2002 (Rosa, 2002). General Electric (GE) and International Climbing Machines (ICM) have developed a remote controlled wall climbing robot with a wireless high resolution video camera attached to its back to capture blade surface images. Fraunhofer Institute for Factory Operation and Automation IFF also developed a robot called RIWEA that can register any crack and delamination in the material with exact positions (Fraunhofer IFF, 2013). Both of these robots require post image processing. The literature has not addressed the degree to which a crack can be recognized by image processing. Both of these methods are still under developing or testing and the cost is not clearly addressed at this time. Another disadvantage is that these robots cannot capture images while wind turbine blades are rotating.

Blades Surface Flaws

Typically, in-service WTBs have surface flaws in the following categories.

1. Erosion (leading edge erosion, also called pitting and wear)
2. Cracks (Cracks in gel coat/channel cracks, stress cracks)
3. Skin debonding (paint peeling, gel coat cracking, and gel coat/skin debonding)

The gradual destruction of wind turbine blade surfaces is called erosion. Erosion is caused by rain, sand, or other natural agents and it affects paint, gel coats, and fiberglass lamination. Typically, erosion appears as a group of small pits, which have a different (darker) appearance compared to a healthy blade surface. Mathematically, these pits have depth and differ from other surface roughness like dead insects which raise the surface of a blade. However, erosion is difficult to recognize in point cloud format due to noise and the current state of image processing technology. Ideally, computer-aided image processing should be able to detect erosion by identifying pitting geometry and luminance.

Cracks become visually apparent as segments along the WTBs where the surface has split without breaking into separate parts. Various industries have tried to observe and characterize surface cracks. “Cracks usually have low luminance and can be considered as local intensity minima with rather elongated structural characteristics (Giakoumis, 2006).” It is critical to determine whether the crack is in the surface coating, like a scratch, or whether the crack affects inner laminations. Therefore, the crack inspection method in the paper needs to address how depth of a crack reflected in a two dimensional image. An effective crack inspection method must be able to distinguish between cracks in paint/gel coat and cracks affecting inner laminations.

Many early defects are hairline thickness cracks along the gel coat layer. Gel coat cracks have various forms that can be found at the root section of the rotor blades, or along the leading edge and surfaces along the spar cab. Gel coat cracks can have a single cause and multiple causes.

Stress cracks, also called linear cracks, usually happen when the laminate flexes under load and generally show up as parallel or concentric lines as shown in Figure 2. Stress cracks can be parallel or traveling towards the same ending point.

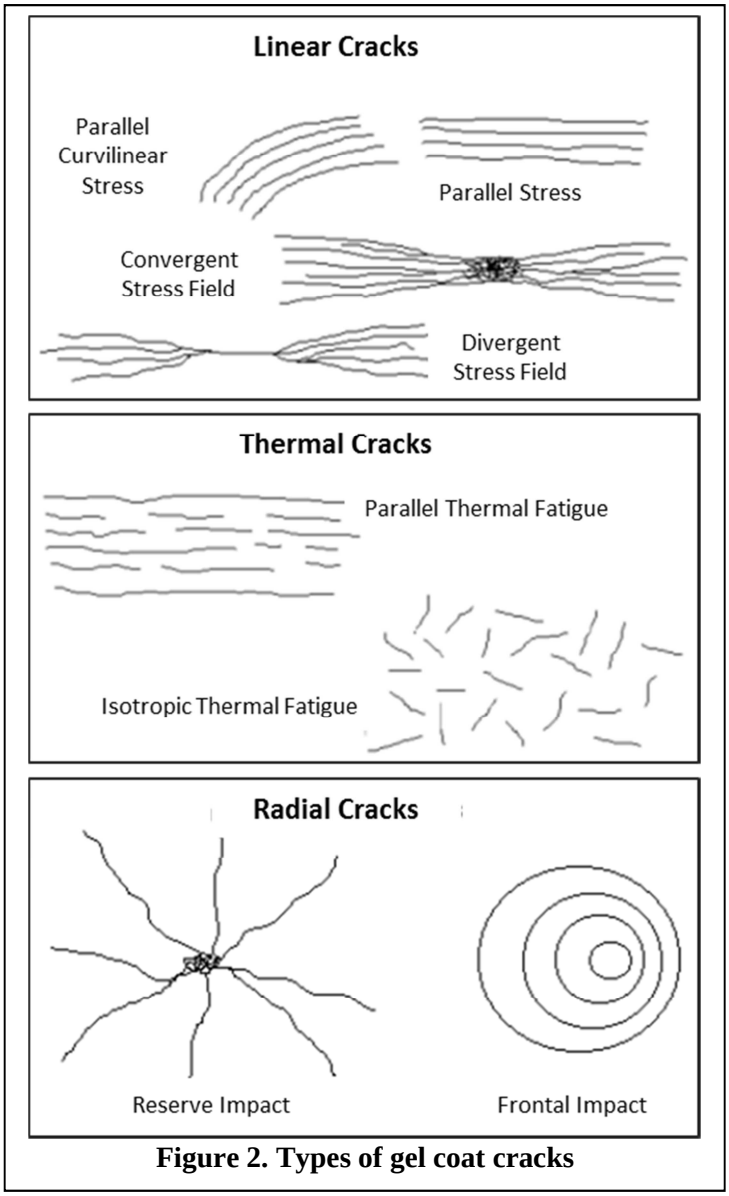

Figure 2. Types of gel coat cracks

Thermal cracks developed in random directions. Aging or a gel coat layer that is too thick can exhibit this problem. Some researchers recognize thermal cracks are a result of repetitious expansion and contraction of the gel coat form. It can be in a parallel pattern or an isotropic configuration and it is characterized by short discontinuous sections. Early thermal cracks can be considered as a material or manufacturing problem.

Radial cracks, also known as crazing or impact damage, typically occurs when an object hits the laminate and causes damage like that shown in Figure 2. The frontal impact is

indicated by a concentric circle pattern, with the diameter of the inner circle having a relationship to the size of the impacting object.

Debonding is a failure mode in which bonding resin is removed and the two bonded layers of materials are separated. Debonding occurs in both the surface coating and inner composite lamination. Skin debonding refers to the coating of the wind turbine blade surface. It can be top paint peeling and gel coat/skin debonding. Paint peels usually have a polygon shape and can be mathematically represented in the image processing. However, paint peeling and gel coat/skin debonding more likely occurred in composited made boat rather than wind turbine blades (Coackley, 1991).

Computer-based Visual Inspection and Challenges

Visual inspection is used to inspect commercial aircraft surfaces for defects. An aircraft surface inspection is typically composed of 90% visual inspection and 10% Non-destructive Inspection (NDI) (Siegel, 1997). NDI is a well-accepted method for finding internal defects in composites. Image-based surface inspection can be used to determine whether NDI is necessary or not. Currently, inspection methods depend heavily on human eyes, which can be time consuming and have poor accuracy. Remote visual inspection tries to address these issues.

Mumtaz described a mobile inspection unit called the Crown Inspection Mobile Platform (Mumtaz, 2010). This unit combines contourlet transform and discrete cosine transformation to find edges of flaws in the aircraft surface. Countourlet transform can efficiently identify the intrinsic geometrical structure containing contours by filtering discontinuous points. Discrete cosine transformation was used to extract features and to

recognize pattern. Airlines have demonstrated the technology and apparently given it some of approval. However, it has only been tried on a small sample set of simulated cracks. The authors stated that the system must be applied to many new types of cracks and surface issues before it can begin to replace human visual inspections. Based on the crack images in the paper, the author did not address how much detail of a crack can be recognized and how to handle the missing part due to the uneven illumination of the image background.

Some researchers are now trying to develop computer-based visual inspection systems for WTBs to make use of the robot inspection methods explained earlier. WTB surface images tend to have more noises comparing to aircraft since blades cleaning is not as often as aircraft. Also, blade surface images have more uneven illumination due to the large scale, complex geometry, and on-tower inspection.

Image Processing

Image Structure

The synthetic cracks are RGB color images, which are $M \times N \times 3$ arrays of color pixels, where M and N are the width and height, respectively, of the image in pixels. This represents a superposition of red, green, and blue component images. Each matrix element can have a value ranging from 0 to 255, where 255 represents full and 0 represents zero intensity level of a single color. For instance, red color has intensity [255, 0, 0]. RGB color images share the same characteristics as the true images in the MATLAB environment and this indicates that the behavior of image processing of field images should be consistent as the synthetic cracks. Each of the component images can

be interpreted as a gray-scale image, where the gray-scale image is a $M \times N$ matrix of pixels. Converting a RGB image to gray-scale eliminates the hue and saturation information while retains the luminance. Image processing with RGB images are equivalent to process the three component images separately, where gray-scale images contain the key information as RGB images but only requires 1/3 of the work. Therefore, the method first converted an image from RGB to gray-scale. Binary images, which have either a black or white color for each pixel, were also used with the method. Most edge detection functions return a binary image with 1 is where the function finds edges and 0 is elsewhere. Converting a gray-scale image to a binary image requires a threshold number T, which turns every pixel of an image into white if its gray level is larger than T and black in the opposite (McAndrew, p.217). Threshold number is widely used in image segmentation and threshold number is directly linked to the accuracy of the detection method.

Image Segmentation

Segmentation is an image processing method in which the outputs are attributes extracted from input images. Segmentation algorithms for binary images are generally based on discontinuity and similarity of pixels. However, nontrivial images are one of the hardest groups to apply the segmentation processing to since too much noise is generated during the image processing and not enough defects can be recognized due to the non-uniform background illumination. Line detection and edge detection used in the project are typical application of image segmentation. Line detection has four standard detector mask with orientations in horizontal, vertical, +45˚ and -45˚. Edge detection is

by far the most common approach to detect discontinuity and there are various detectors available for computing the gradient like *Sobel, Prewitt, Roberts, Laplacian of a Gaussian (LoG), Zero crossings*, and *Canny. Canny*, as the one of the most powerful method, is applied to the project and compared with *Sobel*.

Gray-scale Image Processing

Gray-scale image can be used directly in edge detection methods since edge functions have steps to convert gray-scale image to binary. Recently, there are methods that directly apply the line detector masks to the gray-scale images and then extract the detected lines from the processed images by selecting pixels with responses are not constant. Constant response means there is no discontinuity. However, if there are intensive small noises in the background, it would be very difficult to extract detected lines from the processed images since there is no constant response. Converting to binary image was used to eliminate the irregular noises in the background. Hough Transformation was also investigated to find the line segments and circles with gray-scale images corresponding to the Hough transform (Tao, 2005 and 2010). However, further study is necessary to consider applying Hough Transformation in crack inspection.

Research Problem

The primary objective of this research is to investigate whether wind turbine blade surface images with known cracks can be detected and if so, how much of the crack can be capture and identified with computer-based visual inspection. To achieve this objective, this research will address three questions, namely: 1) to what extent can

surface cracks be detected on WTBs, 2) how sensitive are these methods to variations in crack parameters, and 3) how can we characterize the severity of the cracks?

CHAPTER 3: METHODOLOGY

Description

The methodology contains four major sections.

1. Sample crack generation: Six representative synthetic cracks were generated and four field images were selected to study the parameters that define detectability.
2. Line detection method: Is it possible to quickly scan a WTB and find cracks?
3. Edge detection method: How much of a crack's detail can be captured?
4. Crack quantification: How does one define the severity of a crack (e.g., size, color)?

Summary

A series of synthetic cracks were generated to understand the common characteristics of a composite surface crack and the factors that define the visibility of a surface defect. The reason why synthetic cracks were used is because the available crack image pool is limited and it is necessary to define the fundamental characteristics of a crack. Brownian motion was used to create a random crack with correlation between neighboring points on the crack. Variations in thickness and color were also included. Line and edge segmentation algorithms were developed to detect hairline and nontrivial thickness cracks. Line detection was applied first to provide the capability of a quick overall scan of images of rotor blade surfaces and then the edge detection method was used to extract smoothing information from the original images. The goal was to define how much detail of a rotor blade's surface defect could be found with digital image processing. In addition to understanding the detectability of the method, it was necessary to understand any potential error that image processing might introduce. A defect quantification algorithm was developed to quantify the recognized surface defects. Finally, the method

was tested on a group of well-selected site images and the findings were addressed in the results section.

Sample Crack Generation

Synthetic Cracks

To understand detectability, a set of representative synthetic cracks was generated with one dimensional (1D) Brownian motion to create samples in a controlled fashion. "1D Brownian motion is composed of a sequence of normally distributed random displacements and their sum represents a particle trajectory in one dimension (EPFL, p2)." The background color of the synthetic cracks was defined as either white or light gray to be consistent with the paint color of a rotor blade. The color of the synthetic crack itself was varied to represent the severity of a crack. The color of surface cracks gradually changes as the cracks go deeper into the surface and become easier to identify in digital images. The complexity of a synthetic crack was reflected in its non-uniform thickness, variation in color, and small derivative cracks.

Difference of intensity level of pixels, irregular distribution and geometry of noises, and uneven illumination of the image background are three major concerns that can significantly decrease the detectability of a crack (Gonzalez, 2004). Also the geometry and color of a crack may have some level of impact on the defect detectability. Therefore, we generated three representative groups of synthetic cracks to test the corresponding three hypotheses listed in Table 1. Synthetic cracks can better represent the random nature of cracks because they are more flexible for manipulating the key parameters of a crack. The only difference between the synthetic cracks in Group 1 is the

intensity level of the pixels on the background. The second group was used to examine if computer-based visual inspections can find defects that are difficult to see with human eyes. The third group explained how much of a crack can be detected if there is severe noise or uneven illumination of the background.

Table 1. The characteristics of synthetic cracks that may affect the detectability

Group number	Hypothesis	Characteristics of the synthetic cracks
1	Different intensity level of pixels of the background of a crack affects its detectability.	The color of the cracks is the same, but the background colors are white and light gray respectively.
2	Computer-based visual inspection can observe small thickness cracks or weak intensity level of pixels that human cannot see.	Same level of color difference between a crack and its background. However, the color of the cracks is different. Same as the background color. One unit thickness.
3	Irregular noise and uneven illumination affect detectability.	Non-uniform thickness of two synthetic crack images. One has irregular noise and the other has uneven illumination

Parameters of the Synthetic Cracks

Six synthetic cracks were created according to the hypothesis in Table 1 to find the factors that define the ability to detect surface cracks of a wind turbine blade by digital image processing. The goal of the synthetic curve design was to represent the parameters of a crack and to reflect the parameters of the method that may affect the detectability. Each group contains two synthetic cracks and all of them have the same image size. All of the synthetic cracks have the same starting points at the origin of the coordinate system (0, 0). However, the starting point can be selected by the user in the algorithm.

For the first group shown in Figure 3, one synthetic crack has a white background with RGB values of [255, 255, 255] and the other one has a light gray background with RGB

values of [211, 211, 211]. Both of the cracks have the same gray color [190, 190, 190] with a uniform thickness of three pixels. This group of samples addressed some of the effects of background color on image processing results.

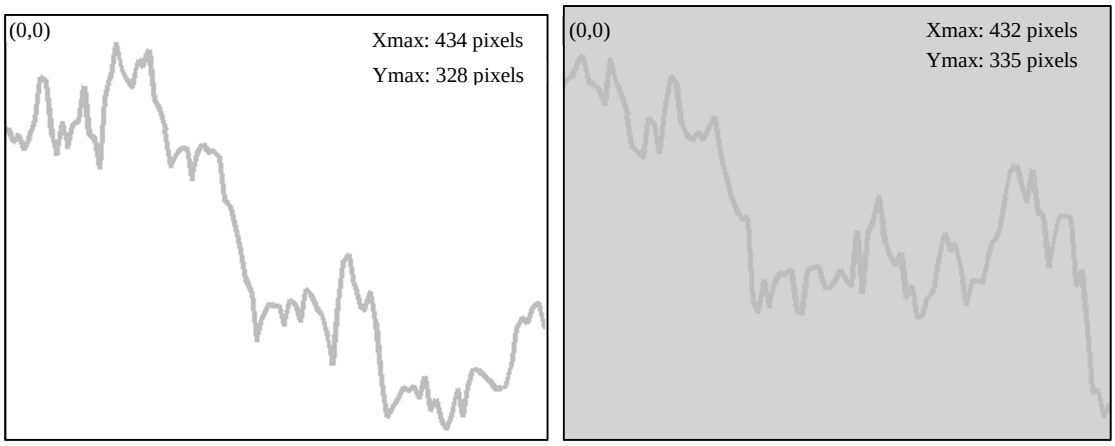

Figure 3. Different intensity level of pixels of the background of two synthetic cracks (a)|(b)

In the second group shown in Figure 4, the background colors of the two synthetic cracks are white and light gray, the same as in the first group. The image with the white background color has color index [234, 234, 234] for its cracks and the other one has color index [190, 190, 190] for its cracks. The numbers were selected to generate hairline cracks that have a very small intensity difference from their background and are hardly recognized by human eyes. The purpose of the samples in Group 2 was to understand the relationship between background color and the color of the crack itself. Both of the synthetic cracks in Group 2 have uniform thickness 1, which examines whether the detection method is sensitive to hairline thickness cracks.

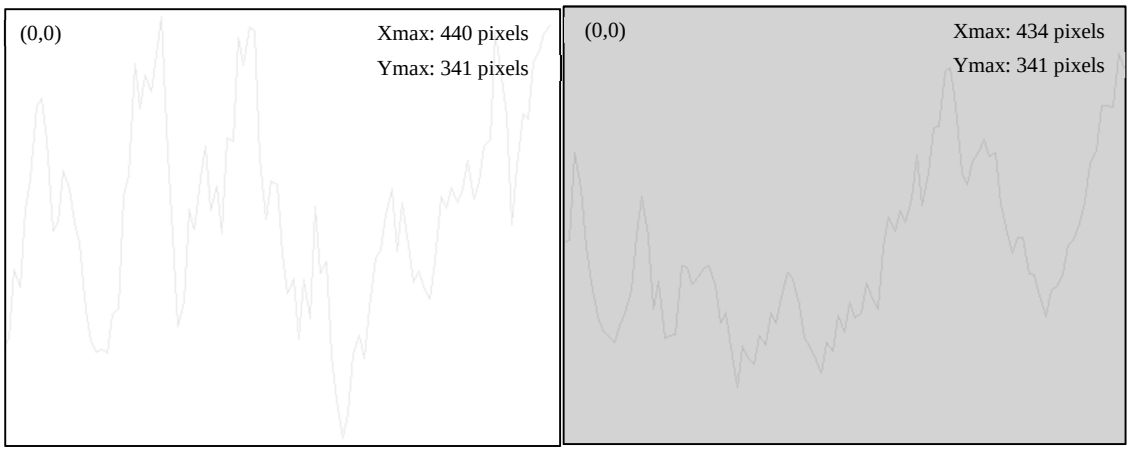

Figure 4. Hairline thickness synthetic cracks with different intensity level of pixels (a)|(b)

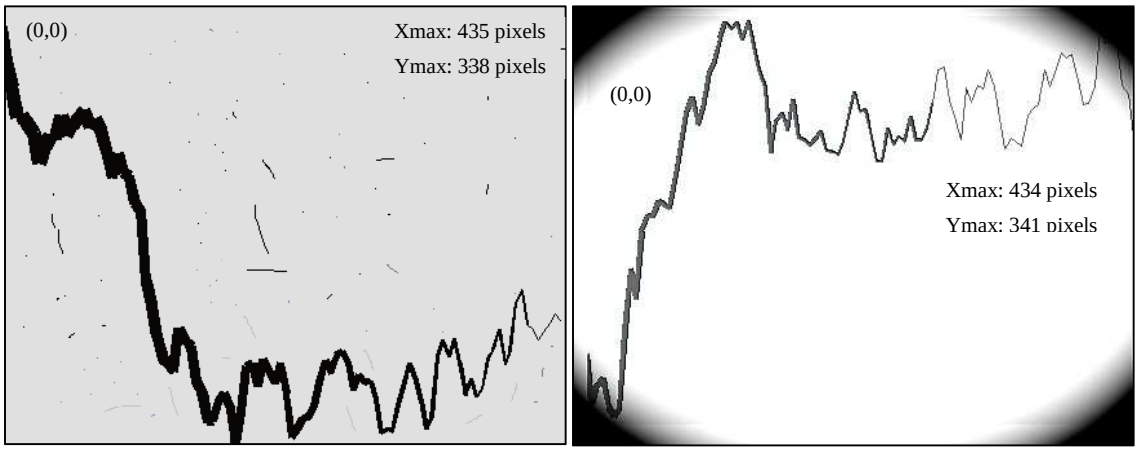

Figure 5. Non-uniform synthetic cracks with (a) noise and (b) uneven illumination

The third group shown in Figure 5 has two non-uniform thickness synthetic cracks with one that has a maximum thickness equal to 9 and the minimum thickness equal to 1. The color of the crack is selected as honeydew [240, 255, 240] to represent a severe crack that goes into the fiberglass lamination. The background color is white with a transparent color from -40% to 20% and irregular noises. After converting the image to gray-scale, the background turned white since the hue and saturation were eliminated. The reason to design a non-uniform thickness/width crack was to determine the relation between the

thickness of a crack and the degree of continuity in imaging processing. The other crack of the group had the same size but contains significant uneven illumination in the background, which cannot be eliminated by transforming the image to gray-scale. These representative synthetic cracks were analyzed using the following methods and their results were compared to the results from field images in the result section.

Representative Field Images

Four field images were selected to further investigate the hypothesis in Table 1 and to evaluate if the parameters that define the detectability are consistent with the six synthetic cracks. After testing the method on the three groups of synthetic cracks, the four field images shown in Figure 6 were used to evaluate the accuracy of the method. The results are compared to the synthetic cracks in the result section to check whether the synthetic cracks captured the basic characteristics of a real crack. Three of the field images were representative of early gel-coat failures and the last one was a severe crack along the trailing edge that could be considered as debonding. One was a hairline crack and was recognized as the most difficult flaw to detect with the human eye. The hairline cracks shared the same characteristics as the synthetic cracks in the second group. The second image was a stress crack. It was used to understand the impact of uneven illumination to the detectability of an image. It was also used to address the importance of the direction of the line detection masks. A third crack was crazing, which typically has a spiderweb geometry and some of the small cracks in a crazing may not follow along the four directions of standard line detectors. The second and third images evaluated whether the uneven illumination and noises affected the detectability of an

image as the synthetic cracks in the third group. In addition, the first two crack images had turbine blades painted in light gray and the last one had white turbine paint, which indirectly explained why it was necessary to have the synthetic cracks in the first group.

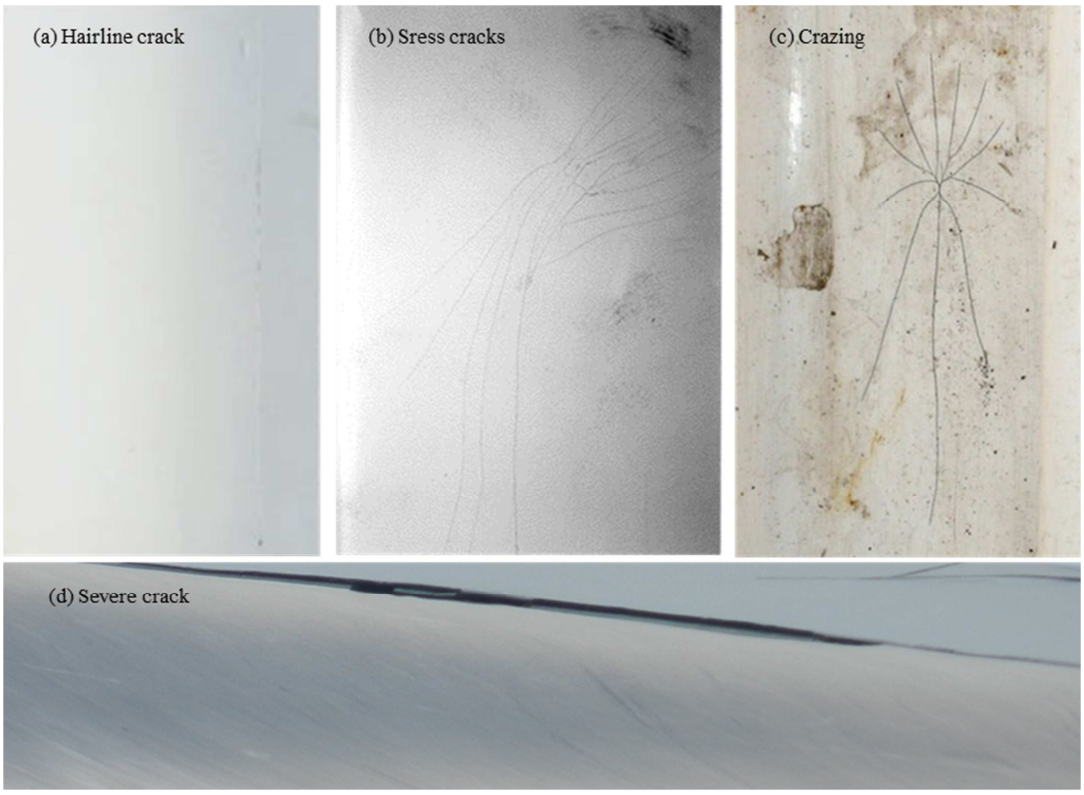

Figure 6. (a) Hairline crack (RGB image: 157-by-272). (b) Stress cracks (Gray-scale: 247-by-350). (c) Crazing (RGB image: 270-by-435). (d) Severe crack (Gray-scale: 573-by-2673).

Line Detection

Line Detector Masks

A line detection method was used to perform a quick scan that could be used on a large scale wind turbine blade. It is simple, fast, and sensitive to individual line segments. Cracks can be treated as a set of segments. A line is a basic type of intensity discontinuity in a digital image and the most common method to detect them is to process the image with a linear spatial filter mask with a binary format as shown in Figure 7. The process consists of moving the center of the mask from point to point in an image and computing the response at each point, which is the sum of the product of the mask coefficients and the corresponding neighborhood pixels lies in the area spanned by the mask and is given by

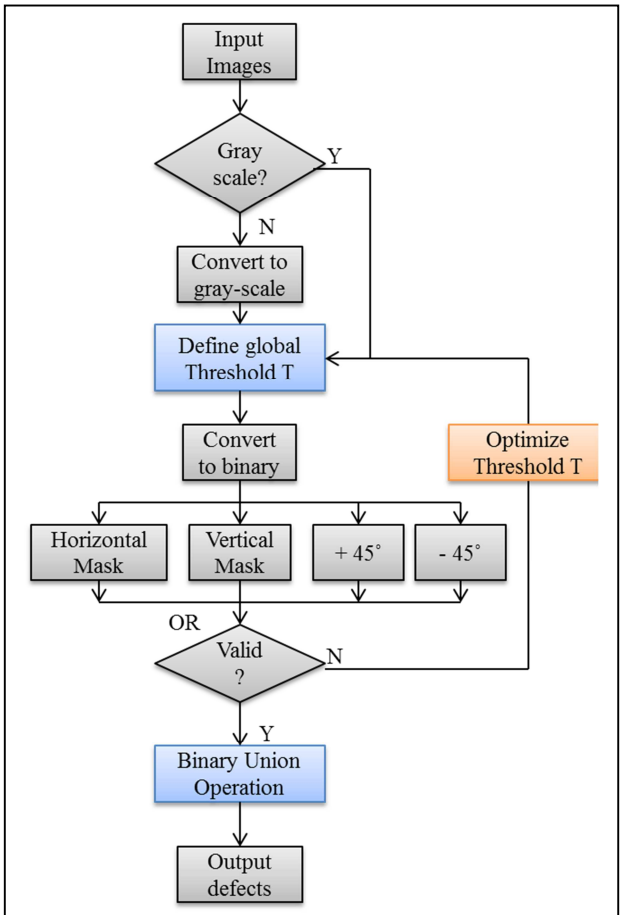

Figure 7. Schematic of quick line detection

$$R = \sum_{i=1}^{n} w_i z_i$$

where, z_i is the intensity of the pixel associated with the mask coefficient w_i.

Theoretically, only an odd number length of masks is considered since R is the response from the center of the filter mask at a specific point(x, y). The smallest mask is a 3×3 matrix and there are four standard line detection masks corresponding to the orientation of the lines, namely, horizontal, 45˚, vertical, and -45˚. The larger number – 2 – in the mask matrix represents the direction of the mask and it has a strong response to one pixel thickness segments. For instance, the vertical line with thickness one is the strongest after filtered with mask in Figure 9 (d).

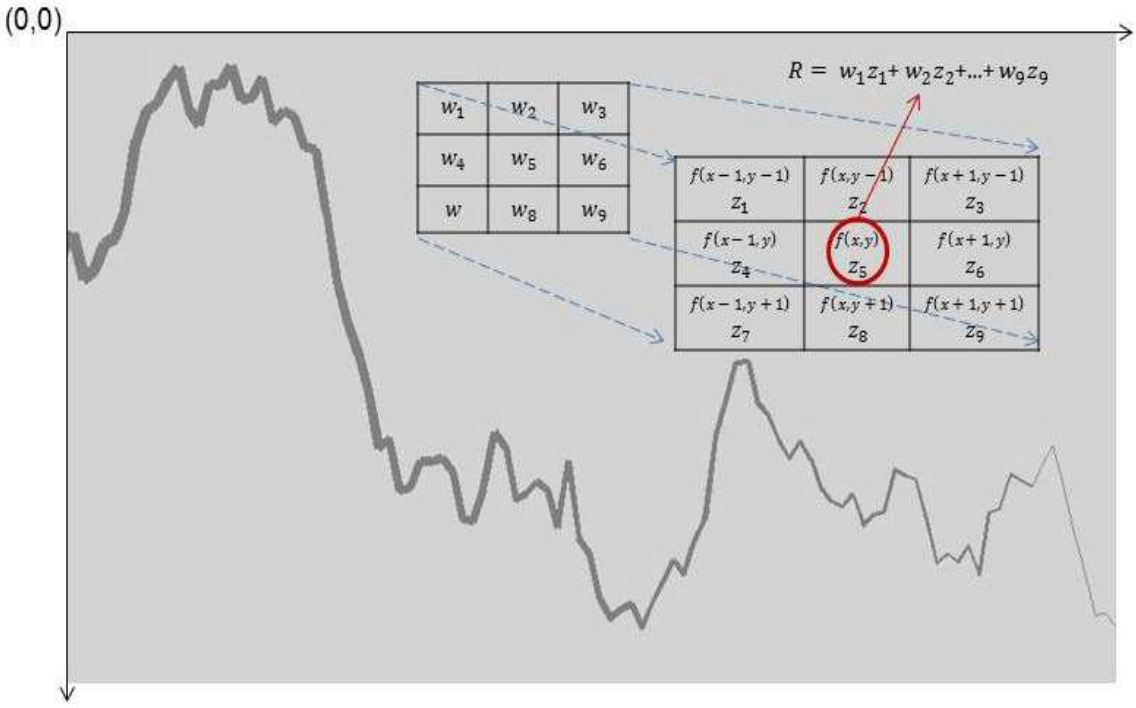

Figure 8. The mechanics of linear spatial filtering. The magnified drawing shows a 3×3 mask and the corresponding image neighborhood directly under it (Gonzalez, p90).

Increasing the number from 2 to 3 smoothed the output image but continually increasing the number will create fuzzy results. Although the vertical line detector masks responded strongly to one pixel thickness lines, it can recognize all vertical lines with different thicknesses as shown in Fig 9 (b).

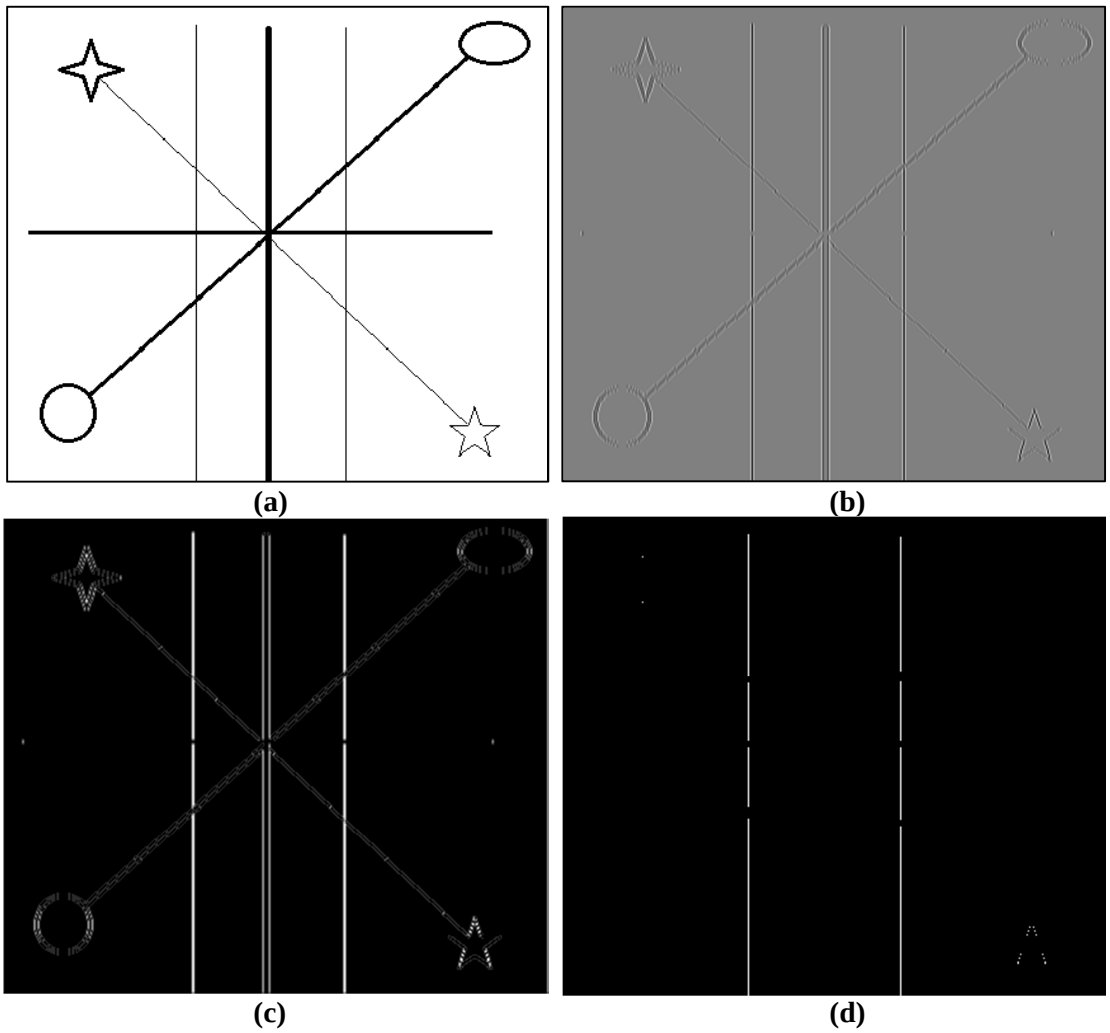

Figure 9. (a) Original image. (b) Result of processing vertical mask in Table 2. (c) Absolute value of (b). (d) Strongest response with g>=T, g is the response at each pixel of the original image

Table 2. Standard line detector masks (a) Horizontal. (b) 45˚. (c) Vertical. (d) -45˚

-1	-1	-1
2	2	2
-1	-1	-1

2	-1	-1
-1	2	-1
-1	-1	2

-1	2	-1
-1	2	-1
-1	2	-1

-1	-1	2
-1	2	-1
2	-1	-1

The binary union operation in Figure 7 combines the detection results of the four standard line detector masks, which can offer more complete results. The standard line

detector masks have a response equal to zero if the mask is in areas of constant intensity. Otherwise, the strongest response represents the direction of a detected line. In the line detection algorithm, images were converted to a monochrome format and then the four different masks were applied to the image. There were four responses $|R_1|$, $|R_2|$, $|R_3|$, and $|R_4|$ with respect to the four line detector masks. The largest response of a point in the image defined the orientation of a line passes the point such as it is vertical if $|R_3|$ has the largest return value. Mathematically, $|R_i| > |R_j|, \forall j \neq i \ \& \ i, j \in \{1, 2, 3, 4\}$ had the line direction as i mask.

The line detection mask elements shown is Table 2 are standard line detection masks and have strong response to one-pixel thickness lines. By changing the mask value, it will give a different response to the thickness of a crack. By multiplying 2^n to the standard vertical mask and obtain new detection masks as in Figure 10 (a) and (b), the strongest responses were happened on thicker lines, then reached an optimal number, and returned to same results as the standard vertical mask but much more fuzzy.

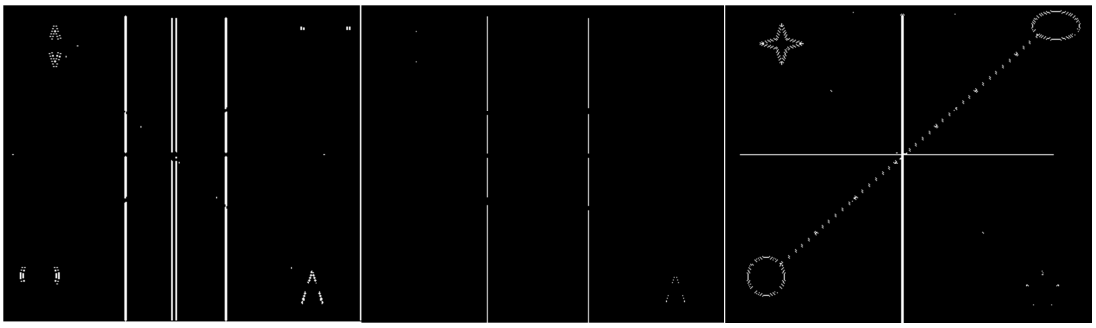

(a) **(b)** **(c)**

Figure 10. (a) All three vertical lines have strong response (b) As Figure 9 (d) but smoother. (c) Middle line has the biggest thickness.

-4	8	-4
-4	8	-4
-4	8	-4

-8	16	-8
-8	16	-8
-8	16	-8

-1	3	-1
-1	3	-1
-1	3	-1

Therefore, standard line detector masks are well-suited to this goal since they have strong response to 1-pixel thickness cracks and can detect the other cracks as long as they are along the direction of the mask within 3X3 neighborhood.

Binary Union Operation for any Possible Direction of Cracks

What if there was part of a crack (thickness < 3 pixels) in the image that was not oriented the same as the four masks above? Then it is complex to have line detector masks for every possible direction of lines. However, one method is to rotate the image counterclockwise with a user defined step size while keeping the masks stationary, say 1˚. After line detection, we can rotate the image back to its original orientation and take the union operation, which maps the detected flaws from each rotation step to one united matrix. Therefore, the line detection method will be able to detect more defects that were limited by the direction of line detector mask. The change to Figure 7 can be seen in Figure 11. However, rotating an image in a very small angle will significantly knock down the detection speed. Based on experience, 10˚ is a reasonable step size that can capture cracks from every direction with a user acceptable fast response.

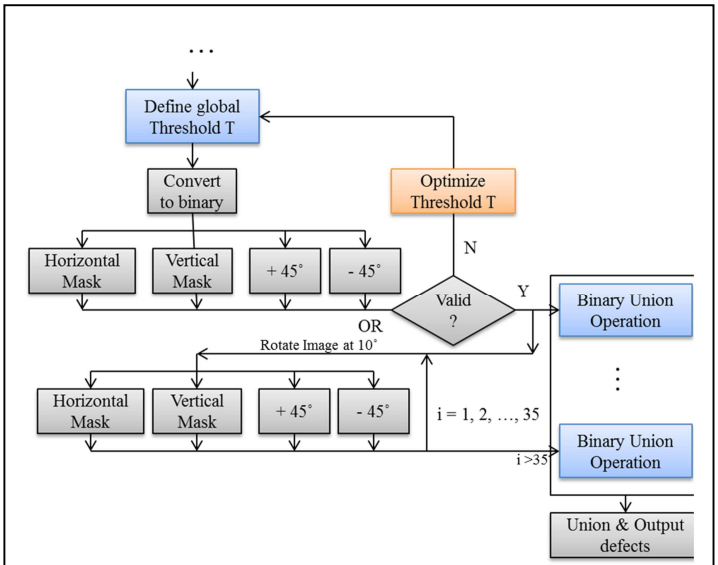

Figure 11. Schematic of updated quick line detection

Optimize Threshold T

A threshold number is used to convert a gray-scale image to a binary image. Suppose $f(x,y)$ is an image and T is a selected threshold number, any point $(x,y) \geq T$ turned to 1 and is called an object point. Otherwise, the point turned to 0 and is called background point. A threshold image $g(x,y)$ is defined as

$$g(x,y) = \begin{cases} 1 \; if \; f(x,y) \geq T \\ 0 \; if \; f(x,y) < T \end{cases}$$

MATLAB toolbox provides a function called *graythresh* that computes a threshold using Ostu's method (Gonzalez, 2004). However, this method tends to generate significant noise when the background illumination is uneven. It was difficult to quantify the size of the crack since the high illumination background became object points and points within the crack became background points.

Noise makes it more difficult to extract the defect information from the original image and it is one of the major concerns in line detection. Both line and edge detection methods have difficulty finding the "optimal" threshold number when the image has an uneven illumination background. Opening image is one way to eliminate the uneven background.

Opening Image – reducing uneven illumination

An opening image is a transformation that extracts the major object from the image and subtracts the leftover non-uniform illumination background from the original image. It is used to reduce the uneven illumination on the background of an image, which typically cause failures of computing threshold number. MATLAB function $strel$ was used to construct structuring elements such as a line or a disk. It had two input variables: shape

and parameters, where shape is a string specifying the desired shape, and parameters are a list of parameters that specify information about the shape, such as its size (Gonzalez, p. 342). The line detection algorithm used line as desired shape. A line shape created a flat and linear structuring element with specified length and direction. For instance, $strel('line', 10, 90)$ returned a flat, linear structuring element that exceeds $\pm$ 10 pixels along vertical direction. If the image is rotating, then one can keep the line structure elements of *strel* stationary. One easy way is to fix the degree parameter of $strel$ to 0 degree and to rotate the detecting image 10 degrees each time counterclockwise as line detecting algorithm in Figure 11. Thus we can extract lines exceeds $\pm$ 10 pixels in most directs. Then subtract the opened image from its original with function *imtophat* and *imbothat* in MATLAB. A comparison of before and after opening image with line detection methods will be addressed in the results section. Opening image does not improve the results very much for edge detection method *canny* that is because *canny* is based on more complex algorithm which will be explained in the edge detection section.

Edge Detection

One major advantage of edge detection is no evidence that the uneven illumination will noticeably decrease the detectability. Edge detection was used to capture the outer contour of non-uniform thickness cracks and to complement the inadequacy of line detectors for detecting meaningful discontinuities in intensity values. Unlike line detection, edge detection uses first- or second-order derivatives to compute the maximum rate of change of gray levels of pixels. Edge detection gave much smoother results while eliminating noise (or small hairline cracks) that probably will miss one

pixel thickness hairline cracks. Therefore, line detection was applied first so that a quick overall scan of images of rotor blade surfaces can be performed in a reasonable amount of time and then the edge detection method was used to extract smoothing information from the areas identified by the line detection.

Edge detection has the same steps as linear detection in Figure 7 except for using edge detection masks, rather than using standard line detection masks. The third group of synthetic cracks had non-uniform thicknesses and noises along the background. Edge detection was used for both of the synthetic cracks and the results were compared to line detection in the result section.

Edge Detector Masks

Edge detection is by far the most widely used method in image segmentation. MATLAB has function, *edge*(), that supports several common detectors: *Sobel, Prewitt, Laplacian of a Gaussian (LoG),* and *Canny*. The key difference between these methods can be found in how the first or second-order derivatives are approximated. The first order derivative in image processing is called *gradient* and is a vector for a 2D function $f(x,y)$ given by

$$\nabla f = \begin{bmatrix} G_x \\ G_y \end{bmatrix} = \begin{bmatrix} \frac{\partial f}{\partial x} \\ \frac{\partial f}{\partial y} \end{bmatrix}$$

with the magnitude of the vector as $g = mag(\nabla f) = [G_x^2 + G_y^2]^{1/2}$ and angle as $\alpha(x,y) = \tan^{-1}(\frac{G_x}{G_y})$, where the angle defines the edge direction. Both the *Sobel* and

Canny methods were considered since *Sobel* is most the commonly used and *Canny* is considered to be the most powerful edge detector. The function *Prewitt* has identical parameters as *Sobel* but with smaller numbers in its mask. Thus, it was slightly faster at computing but tended to produce noisier results. The *LoG* method uses second order derivatives and includes complex steps to eliminate noise and locate the double edge detected by the *Laplacian* method.

The edge detectors *Sobel* and *Canny* were used in the project due to their ability to capture discontinuities and eliminate noise. The *Sobel* function had default masks as shown in Table 3 to compute the gradient of a 2D function, which is composed of vectors G_x and G_y, which were given by

$$G_x = (z_7 + 2z_8 + z_9) - (z_1 + 2z_2 + z_3); \text{ and } G_y = (z_3 + 2z_6 + z_9) - (z_1 + 2z_4 + z_7)$$

where, $z_1, ..., z_9$ are values of pixels in the image that span the *Sobel* masks.

Table 3. *Sobel* detector masks (a) Vertical. (b) Horizontal

-1	-2	-1
0	0	0
1	2	1

-1	0	1
-2	0	2
-1	0	1

It is complex to change the mask number here since each of the gradient algorithms has its own detection masks and cannot be changed easily as line detection masks. Also it is not necessary to update the maskers since the detected results of all ten samples show positive results in the results section.

The *Canny* method is more complex and includes a Gaussian filter, a local gradients and edge directions computation algorithm, and provides edge linking by incorporating the

weak pixels that are 8-connected to the strong pixels. If the user does not select a threshold number, the *Sobel* and *Canny* methods will generate a threshold number automatically, where the threshold of *Sobel* is a number and the threshold of *Canny* is a two element vector.

Optimize Threshold T

The default threshold number generated by *Sobel* or *Canny* does not guarantee a positive result. However, both of them offer promising results by optimizing the threshold value. The *Sobel* method offered less noisy results compared to *Canny* but also tended to miss a significant number of the defects, where *Canny*'s noise tended to be small contours. By updating the threshold number, *Canny* offered the smoothest result, where *Sobel* does not reduce background noises very much by changing the threshold number. However, this required a lot of human intervention, which is not the goal of the research. In the project, the default threshold number was used first and then updated the threshold number with a fixed rate. Apply

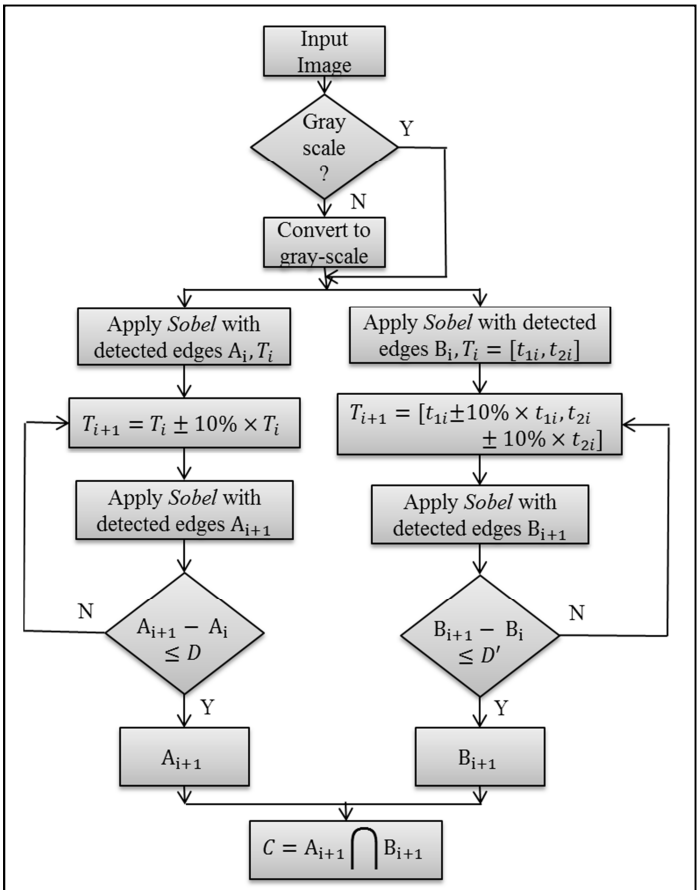

Figure 12. Schematic of edge detection for detailed defects

the edge detection method again and compare with the previous detecting results to see if the difference is within an acceptable tolerance. For instance, the default threshold value of *Canny* method is $T = [t_1, t_2]$ and the results is a matrix A contains all the detected edges along the cracks. Update threshold value to $T_1 = [t_1 + .1 \times (t_2 - t_1), t_2 - .1 \times (t_2 - t_1)]$ and apply *Canny* again with results A_1.Repeat the routine until $A_{i+1} - A_i \leq D$, where D is the tolerance as shown in Figure 12. Both *Sobel* and *Canny* have recognizable edges. Since the major differences between *Sobel* and *Canny* were the amount and geometry of noise, one possible approach was to take the binary interaction operation of the detecting results of *Sobel* and *Canny* to obtain smoother results. However, it did not eliminate very much noise.

Quantifying the Size of a Crack

Two methods were used to quantify the magnitude of a crack. The first and also the easiest way was to find the minimum enclosing rectangle (parallel to the x and y axes) that enclosed the points along the crack. This defined the most likely required repair area. However, it did not give any further information about the orientation of the crack and tended to overestimate the magnitude.

The second approach was to define the minimum enclosing rectangle that was not oriented with respect to the x and y axes. This could be found by estimating the parameters of a line that minimizes the maximum distance to all the points on the crack edges. Using the start and end points of the line by finding the end points on the edges along the line, the sides of the rectangle are found by projecting the end points onto the estimated line. The other two sides are determined by the maximum deviation of the

crack on each side of the line. In order to minimize the maximum distance to the line, the function *fminimax* in MATLAB was selected to find the best fit parametric line, denoted by $\begin{cases} x = at + b \\ y = ct + d \end{cases}$. The function, *fminimax*, requires an initial guess for the parameters of the line [*a, b, c, d*] and a function that computes the maximum distance of all points along the edges to the given line. The function stops when the values of [*a, b, c, d*] are within a specified tolerance (i.e., there is no change) or reach the maximum number of iterations. The default iteration limit is 500 in MATLAB. In this study a limit of 2500 iterations was used.

Two Kinds of Errors

Computer-based crack detections methods make two kinds of errors: false-positive identification of cracks (Type 1) and failure to detect existing cracks (Type 2). One kind of error occurs when a crack is detected but does not exist (i.e., a Type 1 error). This can be caused by noise, which cannot be totally avoided. If the noise is significant, then it is difficult to quantify the crack accurately. The other one is missing defects (i.e., a Type 2 error). In other words, the defects or part of a defect is not recognized with the line and edge detection algorithms. This could be due to high non-uniform illumination of the image background. The consequences of a Type 1 error in this context are not as severe as the Type 2 error, since missing defects can lead to ignoring the necessary maintenance, leading to future structural damage. Type 2 error can be reduced significantly by adjusting the threshold number and by applying binary operations to the results of line and/or edge detections.

CHAPTER 4: RESULTS

Description

The answers to the questions in the methodology chapter are listed below.

1. Noise, the intensity level of pixels, and uneven illumination are major parameters that affect detectability.
2. Line detection method is suitable to quickly scan a WTB and find cracks since it minimizes Type 2 error.
3. Uneven illumination is not a major factor in edge detection methods. *Canny* offers the best results in reducing both Type 1 and Type 2 errors.
4. The severity of a crack is difficult to quantify. However, the crack span size and intensity level of pixels offer important insights on the magnitude of a crack.

Summary

The ten samples, six synthetic cracks and four representative filed images, were tested with both line and edge detection methods. Although there is a tradeoff between false-positive identification of cracks (Type 1 Error) and failure to detect existing cracks (Type 2 Error), *Canny* had the best results by far in terms of reducing the two types of error. Generally, uneven illumination has much less influence on the detectability of edge detection methods compared to line detection. For a very bright background, edge detection offered much better results as shown in Figure 14. Unlike line detection, edge detection eliminated low levels of noise and the detected edges were much smoother.

The opening image technique was applied in the line detection method to reduce uneven illumination and the results were poor with gradually changing uneven illumination as seen in the stress crack sample shown in Figure 6 (b). In addition, the line detection method was very sensitive to discontinuity and thus, the detected results had more Type 1 errors as compared to edge detection methods. However, this was not in conflict with

our goals that line detection could be used as a quick scan of the entire turbine and edge detection methods were used to capture the detailed information of the crack. The crack quantification algorithm drew the approximation line with minimized maximum distance to all the detected edges, including noise. Then parallel lines to the approximation line that enclosed all the defects were used to define a bounding box.

Line Detection

With the rotating image and binary union operation added to the line detection method as shown in Figure 11, line detection was able to capture cracks in every direction (not only horizontal, vertical, +45˚, and -45˚) and the staircase caused by the small size of 3X3 detector masks was minimized. Line detector masks are very sensitive to noise and thus, it minimized the Type 1 error but had difficulty with Type 2. The line detection

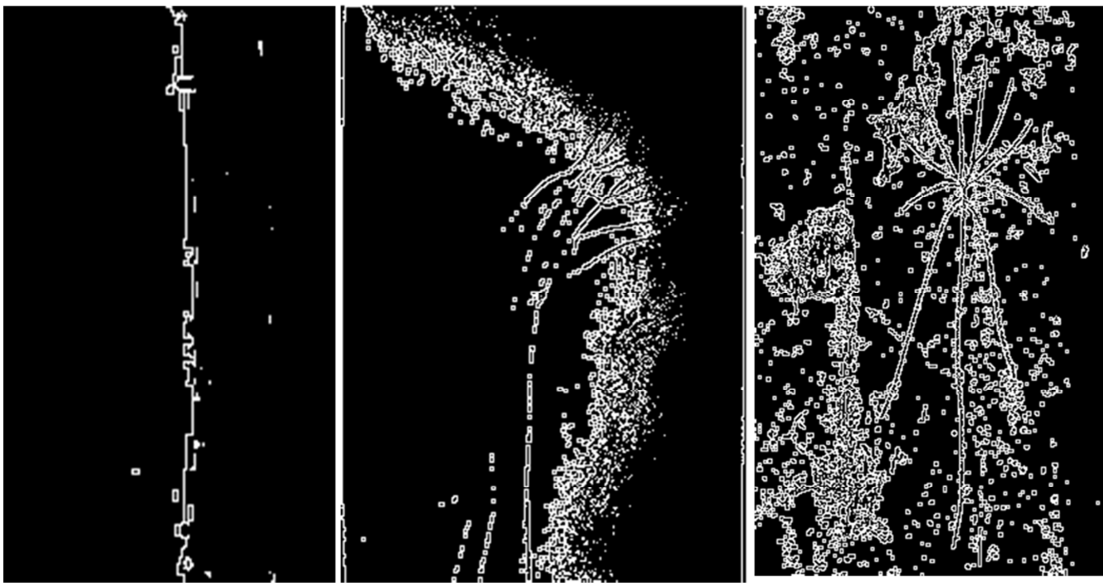

(a) Hairline crack. **(b) Stress cracks.** **(c) Crazing.**

Figure 13. Field sample of line detection

method showed high detectability of the hairline crack shown in Figure 13 (a) with the original image in Figure 6 (a). The hairline crack is very difficult for human eyes to

detect but line detection easily found it. The opening image technique was used to reduce the negative impact of uneven illumination. However, the results were poor, as shown in Figure 13 (b). Line detection had trouble eliminating background noise like dirt on the surface of turbine blades. For this reason it is necessary to apply edge detection methods to the defective areas detected by line detection method.

Edge Detection

Edge detection methods like *Sobel* and *Canny* offered much smoother results compared to the line detection method. Noise and uneven illumination did not have a significant impact on edge detection. The intensity level of pixels is very important to both line and edge detection methods because if the intensity level of noise is larger than the intensity level of the defect, the defect will not be detected since the computer will consider it to be background noise and eliminate it. When testing sythetic cracks with both line and edge detection method, the first two groups and the first four synthetic cracks had the same results. Neither the color or size of the crack affected the result. In other words, both the line and edge detection methods could easily detect hairline cracks. However, both *Sobel* and *Canny* had to adjust the threshold values to detect some cracks. Without the threshold adjustments, *Sobel* and *Canny* had difficulty detecting stress cracks with highly uneven illumination and crazing cracks with noisy backgrounds. With the default threshold value, it is difficult to say which method offered better results as shown in Figure 14 (a-1) and (a-2). That said, *Canny* can significanlty improve its results by optimizing new threshold values. The results under *Sobel*, however, were not improved so easily by changing the threshold values. Since *Sobel* and *Canny* have different

gemoetries of noise, we applied intersection operation to the optimized results in Figure 14. (b-1) and (b-2). The intersaction operation significantly reduced Type 2 error without generating too much Type 1 error.

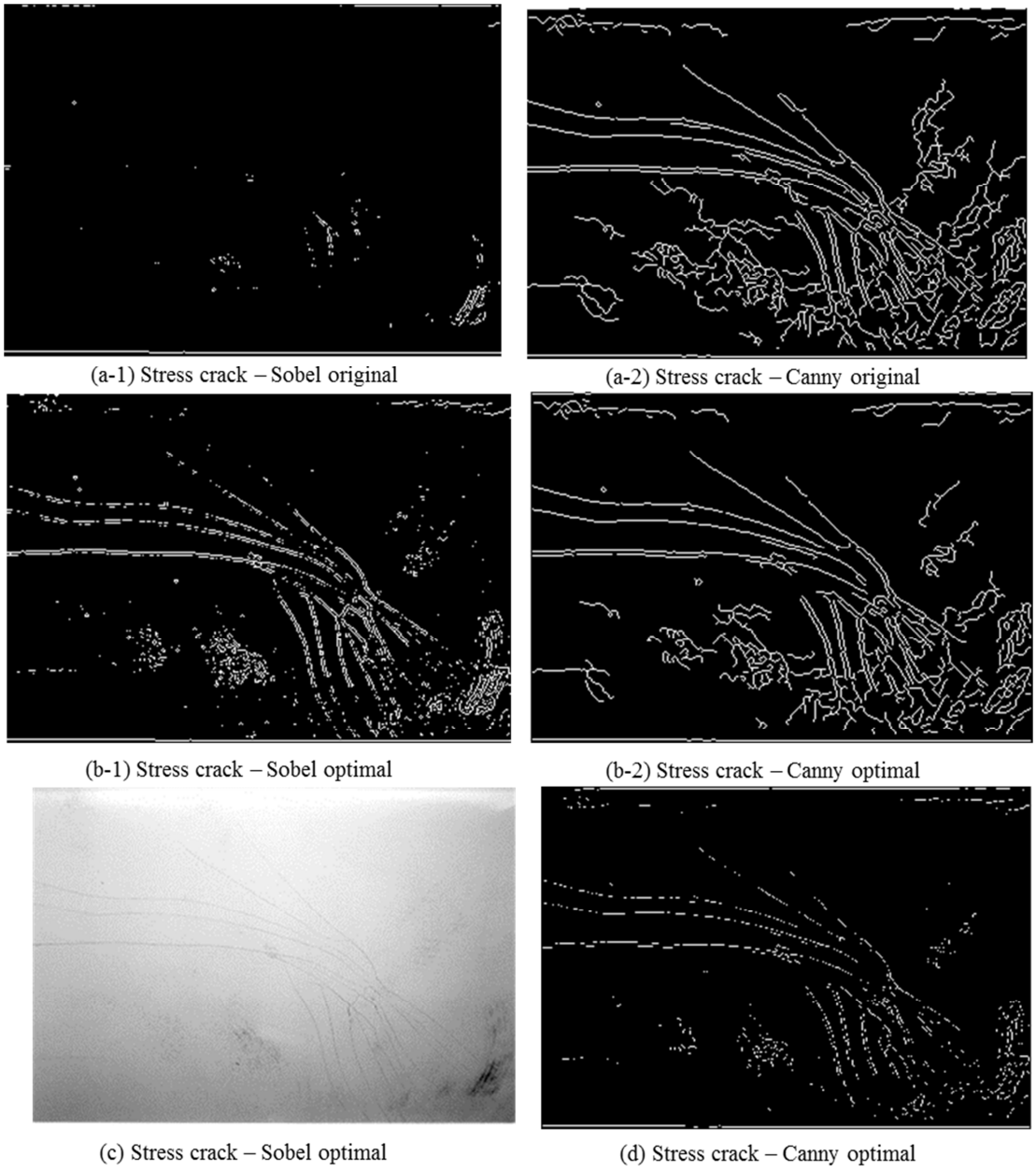

Figure 14. Edge detection reduced uneven illumination significantly

The crazing crack from Figure 6. (c) contains a lot of noise, which is common to rotor blades, especially in a places like deserts with strong wind. Both *Canny* and *Sobel* were able to reduce the background noise impact, which means the computer-based visual inspection method is feasible for onsite application.

(a) *Canny* optimal **(b) *Sobel* Optimal**

Figure 15. Edge detection reduced noises significantly

Factors Affecting Detectability

Intensity level of pixels matter

The first group of synthetic cracks did not show that the method can detect a crack with lighter background color easier than the one with darker background color. When applying the *graythresh* function, the two images resulted in very different optimal threshold numbers. With the optimized threshold values, both of the images resulted in clearly delineated defects. Not surprisingly, the applicable threshold range was significantly different between the two images. The one with a white background had valid threshold number from 0.746 to 0.999. But the one with a gray background had a threshold number between 0.745 and 0.827. Higher threshold numbers were able to eliminate more noise with low- to middle-level intensity from the background, which

can make the results much clearer if there is a lot of noise in the background. However, the tradeoff is that some of the defects can be missed if the defect has a lower intensity level than the noise in the background. One example is shown in Figure 16 with the *Sobel* method. When we selected a threshold value of 0.12, rather than 0.065, most of the cracks and background noises were eliminated because the pixels in the image had an intensity level lower than 0.12 and all of the pixels turned to 0. If the crack had a much higher intensity level than the background noise, then the results had little noise.

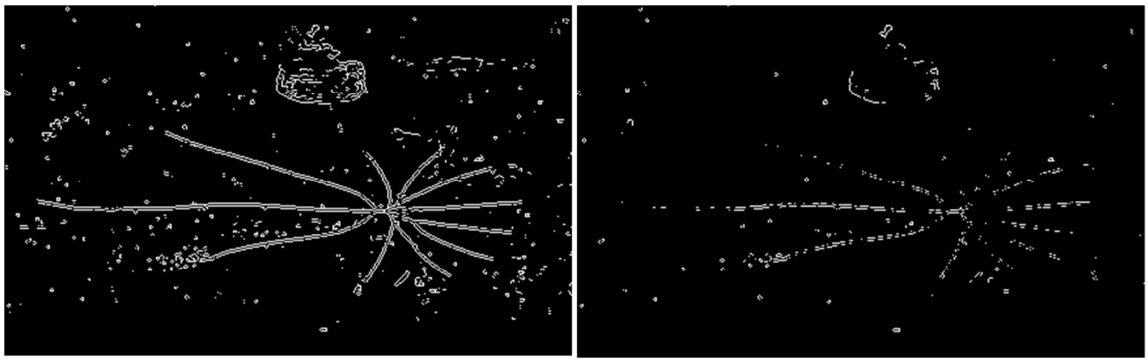

(a) *Sobel* threshold 0.065 **(b) *Sobel* threshold 0.12**

Figure 16. Edge detection affected by intensity level of pixels

Crack thickness is not a factor

Surprisingly, based on both synthetic cracks and field images, crack thickness did not affect the detectability of a crack. The line detection results of the first two groups of synthetic cracks can be found in Appendix A. In addition, Figure 13 shows that computer-based visual inspection method can find small thickness cracks like hairline cracks very easily. These results suggest that the computer-based method may be a better alternative to using sky workers to visually inspect blade surfaces.

Crack orientation is not a significant factor

In the line detection method, images were rotated counter-clockwise with 10 degree increments and then the line detector masks were able to capture lines from most directions. Binary union option mapped all the detected lines into one image as shown in Figure 13 (c). Edge detection methods are based on first- or second- order derivatives, which are not influenced by crack orientation. Therefore, both line and edge detection methods in the project were not affected by crack orientation. In other words, the orientation of the field camera is not expected to affect the results.

Background illumination matters

Automatic threshold computing methods tend to fail when the background illumination of an image is uneven (i.e., there is variance in the pixel values). Uneven illumination had a severe impact on the line detection method as shown in Figure 13 (b), where the opening image technique was applied to reduce the impact of uneven illumination. The opening image technique did not improve the results very much. The original image of the stress cracks in Figure 6 (b) had very bright lighting on the background and the results were poor even after the opening image process. Only one of the three cracks was detected and most of the pixels associated with the cracks were deleted during the opening image process. Therefore, the lighting problem still poses a challenge to reliable crack detection for line detection method. Further research is warranted to reduce the effects of uneven lighting on crack detection. Edge detection method reduces the uneven illumination problem for the same cracks shown in Figure 14. (b-1) and (b-2). This supports the hypothesis we made earlier that it would be most effective to use the line

detection method to do a quick scan and then apply edge detection method to maximize the details of a crack.

Quantifying the Cracks

After the flaws were detected, they were bounded in a rectangle and two parallel lines. The rectangle indicated the recommended repair area. The two parallel lines indicated the direction and magnitude of the cracks. However, if there was a lot of noise, the parallel lines were just the lines parallel to a line with minimized maximum distance to all the points detected, which included noise and very small flaws as seen in the results in Figure 13 (c). Therefore, eliminating noise as much as possible is very important in estimating the magnitude of a crack.

The first synthetic crack in the Group 1 was selected to address the results of quantifying a crack since the direction of the crack is clarity and we can see clearly if the approximation line follows the direction of the crack. Other samples either has the same structure as this one, for instance, cracks in Group 1-2, Group 2-1, 2-2, and Group 3-2 have the similar cleanness or contains too much noise to observe how close the approximation line follows the direction of the crack (see Appendix A). First, the recommended repair area is enclosed in the blue rectangle with 423-by-301 pixels. The original image has 434-by-328 pixels shown in Figure 3(a). An approximation line with minimized maximum distance to all the points along the crack was generated is shown in Figure 17 in green and the parametric function of the green line is:

$$\begin{cases} x = 439.2590 * t + 202.6571 \\ y = 277.2023 * t + 166.7593 \end{cases}$$

where $t \in [-0.46, 0.502]$.

The two parallel lines in red enclosed the cracks with minimum distance to the green line as shown in Figure 17.

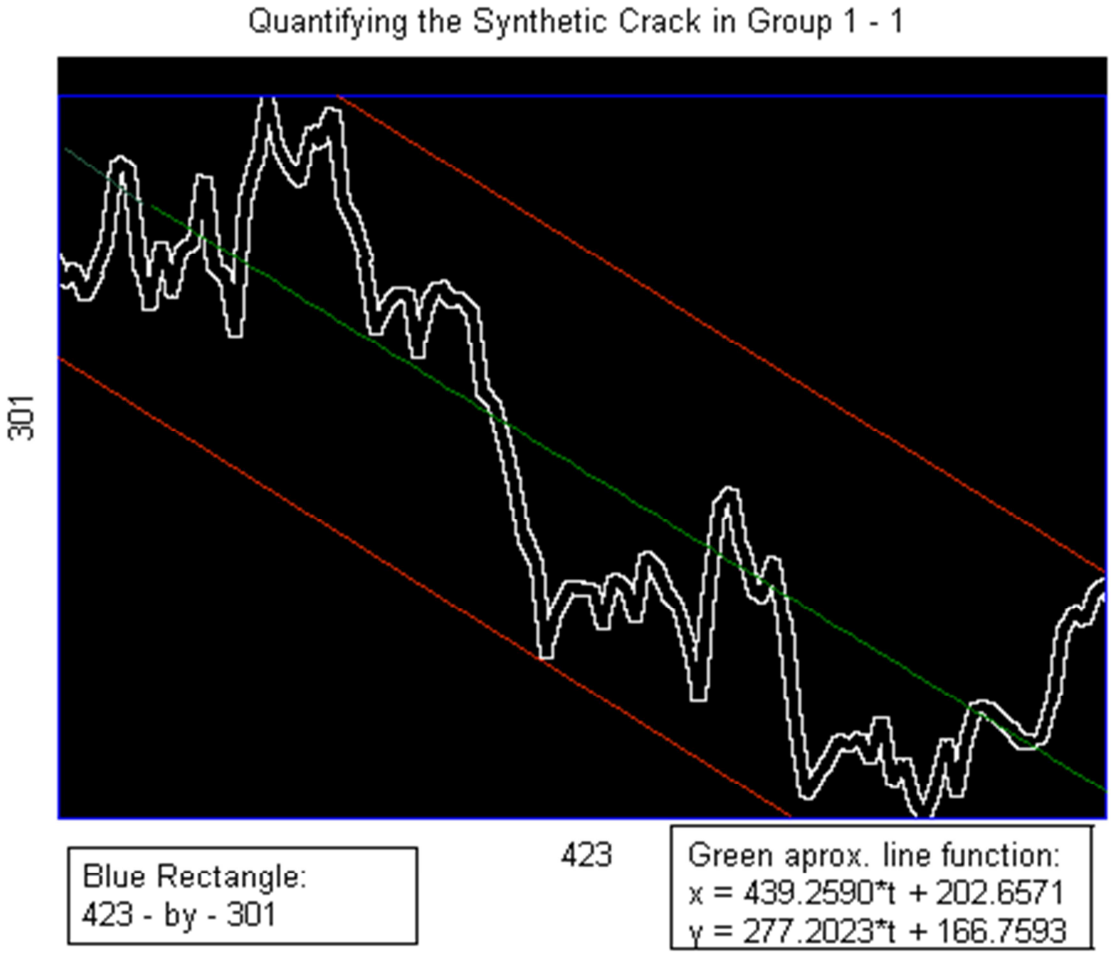

Figure 17. Quantification of the Synthetic Crack in Figure 3 (a)

The severity of a crack was defined by its intensity along the crack and its size. The size of the crack is shown in Figure 17. However, the intensity of the crack is not straightforward since the line and edge detection methods only detected the edges of the crack. Also, the location of the cracks on the WTB can be critical. For instance, if a crack occurred along the leading edge or the root section may create more potential damages or accelerate the potential structural damage than other areas since the leading

edge contacts the wind first and the root section has more accumulation of fatigue loads. However, all of these are hypothesis, which require further study.

CHAPTER 5: CONCLUSIONS AND FUTURE WORK

This paper evaluated two computer-based methods for detecting cracks in wind turbine blades: the line detection method and the edge method. The original hypothesis was that the line detection method would be best for performing a quick scan of the blade surface to find cracks, but that the edge method would provide better data on the crack. The results of the study support our hypothesis.

The line detection method is appropriate for quick scans because it can quickly identify hairline cracks that are invisible to the naked eyes. Image processing thresholds and filters can be used to minimize false-positives caused by surface irregularities like dirt or dust. However, uneven illumination poses serious problems to the line detection method that cannot be overcome.

The edge detection method gives more detailed information about cracks than line detection, but has difficulty distinguishing between surface irregularities and cracks. The most effective method we identified was to first identify the cracks using line detection and only then apply edge detection to collect more information on the crack. Edge detection is particularly useful when there is uneven illumination.

The results showed that computer-based crack detection shows promise for maintenance work on in-service wind turbine blades. With a high quality image and processing tools, computers can consistently identify cracks that are invisible to human eyes, even when looking at the blade from different angles.

Further research is necessary to apply these methods to more sample cracks and to find methods to minimize errors caused by environmental noises like insects.

REFERENCES

Arias, P. and Aresto, J., " Digital photogrammetry, GPR and computational analysis of structural damages in a mediaeval bridge." *Engineering Failure Analysis* 14 (2007) pp. 1444-1457

Chen, A., *New Study Finds the U.S. Wind Power Market Riding a Wave That Is Likely to Crest in 2012*. News Center, Lawrence Berkeley National Laboratory, August 14, 2012.

Coackley, N., "Fishing boat construction: 2 Building a fiberglass fishing boat." Food and Agriculture organization of the United Nations. FAO fisheries technical paper 321, Rome, 1991 ISBN 92-5-103116-9 Reprinted 2005

Elkmann, N., *Robot for the inspection of wind turbine rotor blades (RIWEA).* Fraunhofer Institute for Factory Operation and Automation. Retrieved from http://www.iff.fraunhofer.de/en/business-units/robotic-systems/riwea.html

EPFL, Dept. of Life Science and Technology Section, École Polytechnique Fédérale de Lausanne, Simulating Brownian motion. Retrieved from http://ssv.epfl.ch/files/content/sites/lben/files/users/179705/Simulating%20Brownian%20Motion.pdf

GE Reports, *Go Go Gadget: Robotic crawler rides up 300-foot poles to inspect wind turbine blades.* Jun. 13th, 2012 Retrieved from http://www.gereports.com/go-go-gadget/

Giakoumis, L., "Digital Image Processing Techniques for the Detection and Removal of Cracks in Digitized Paintings." *IEEE Transaction on Image Processing*, Vol. 15, No. 1, January 2006

Gonzalez, Rafael C., *Digital Image Using MATLAB Processing*. Upper Saddle River, New Jersey, Pearson Education, Inc., 2004.

Hahn, B., Durstewitz, M., and Rohrig, K., "Reliability of Wind Turbine – Experiences of 15 years with 1,500 WTs." Institut für Solare Energieversorgungstechnik (ISET), Verein an der Universität Kassel e.V., 34119 Kassel, Germany.

Marsh, G., "Meeting the challenge of wind turbine blade repair." *Reinforced Plastics*, July-August, 2011, Vol.55(4), p.32(5)

McAndrew, A., *Introduction to Digital Image Processing with Matlab.* Thomsion Course Technology, 2004.

Mumtaz, M., "A new approach to aircraft surface inspection based on directional energies of texture." Pattern Recognition, Aug. 2010, pp. 4404-4407

National Renewable Energy Laboratory (NREL) Report, "20% Wind Energy by 2030: Increasing Wind Energy's Contribution to U.S. Electricity Supply." DOE/GO-102008, July 2008

Rosa, Guido L., "A low-cost lightweight climbing robot for the inspection of vertical surfaces." *Mechatronics*, Volume 12, Issue 1, Feb. 2002, Pages 71-96

SGS Group, The cost of wind blade inspections versus blade repair. Hamburg, Germany, Retrieved from http://www.nacleanenergy.com/oldsite/index.php?option=com_content&view=article&id=2327:the-cost-of-wind-blade-inspections-versus-blade-repair&catid=42:feature-articles&Itemid=109

Siegel, M., "Enhanced remote visual inspection of aircraft skin." Robot Institute. Carnegie Mellon University. Proceedings of the Intelligent NDE Sciences for Aging and Futuristic Aircraft Workshop, September, 1997, pp. 101 - 112.

Tao, P., "Detect lines in grayscale image using Hough Transform." December 06th, 2005, Mathworks. Retrieved from http://www.mathworks.com/matlabcentral/fileexchange/9226-detect-lines-in-grayscale-image-using-hough-transform

Tao, P., "Detect circles with various radii in grayscale image via Hough Transform." November 17th, 2010, Mathworks. Retrieved from http://www.mathworks.com/matlabcentral/fileexchange/9226-detect-lines-in-grayscale-image-using-hough-transform

Walford, Christopher A., "Wind turbine reliability: Understanding and minimizing wind turbine operation and maintenance costs." Global Energy Concepts, LLC. Sandia Report: SAND2006-1100 Mar. 2006

Wood, K., "Leading-edge erosion: Materials solutions. Composites Technology." Apr. 1st, 2011 Retrieved from http://www.compositesworld.com/articles/leading-edge-erosion-materials-solutions

APPENDIX

Detection results of sample cracks

Group 1- white background

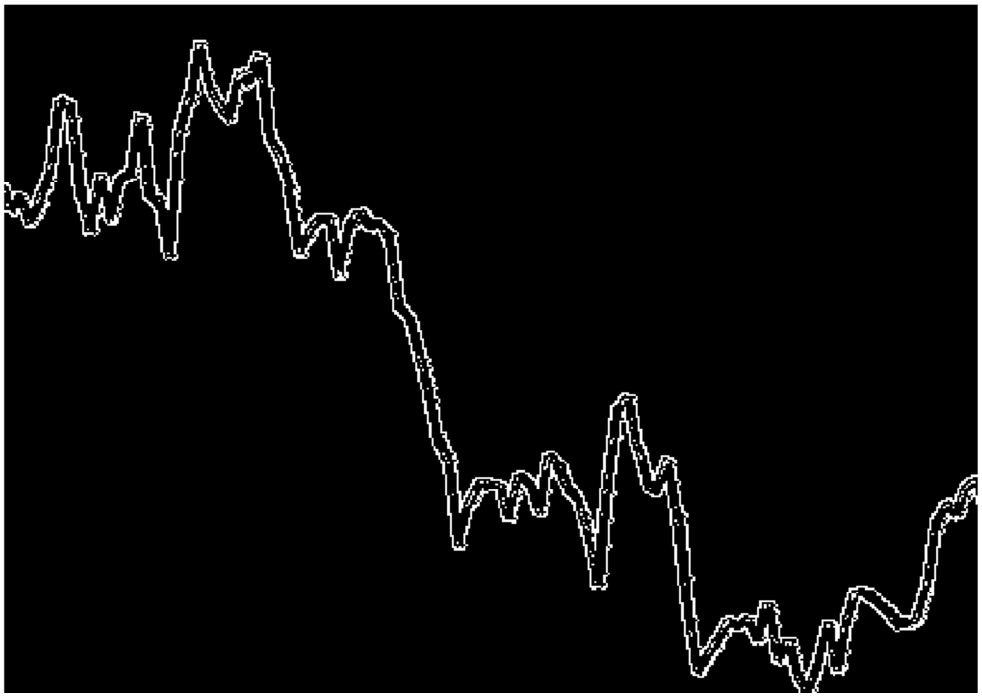

Group1 - light gray background

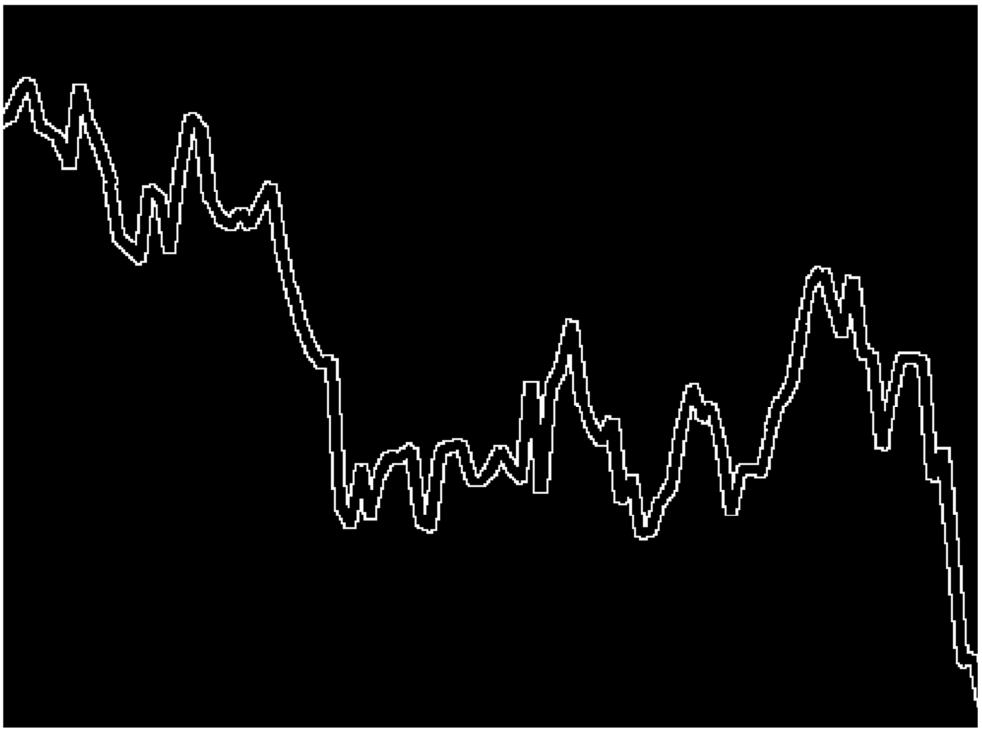

Group 2 - white background

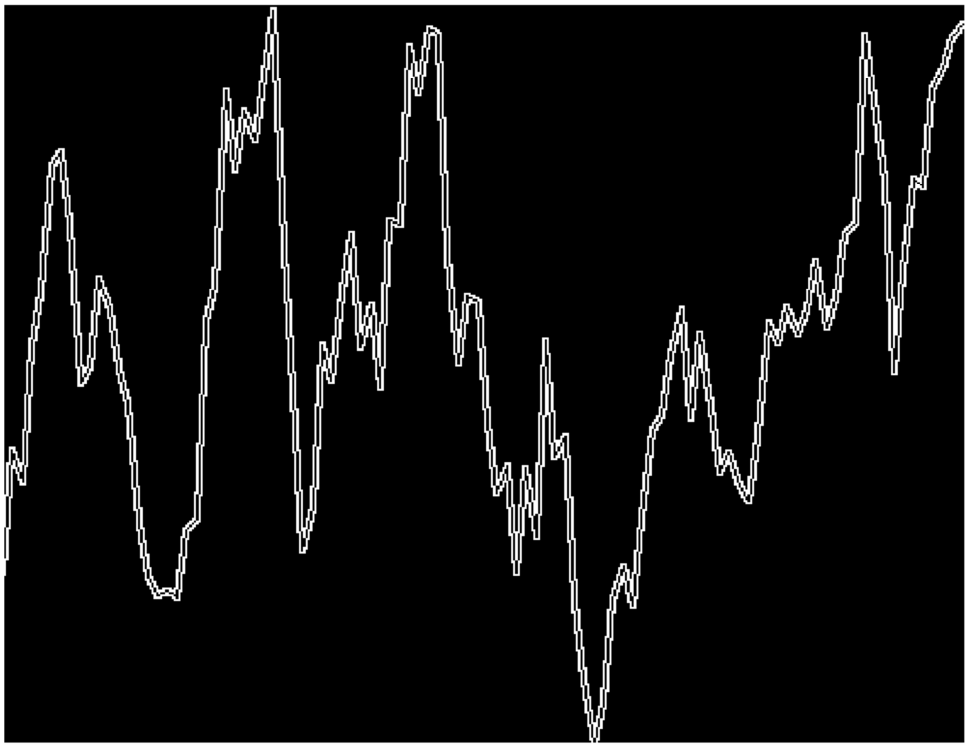

Group 2 - little gray background

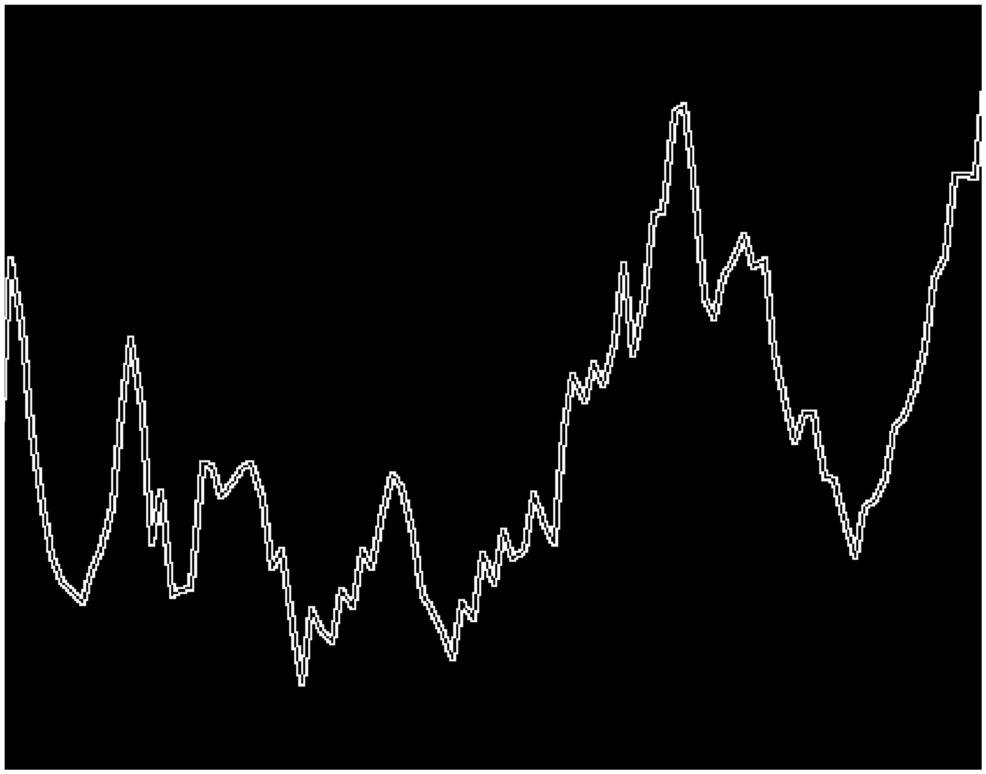

Group 2 - noise

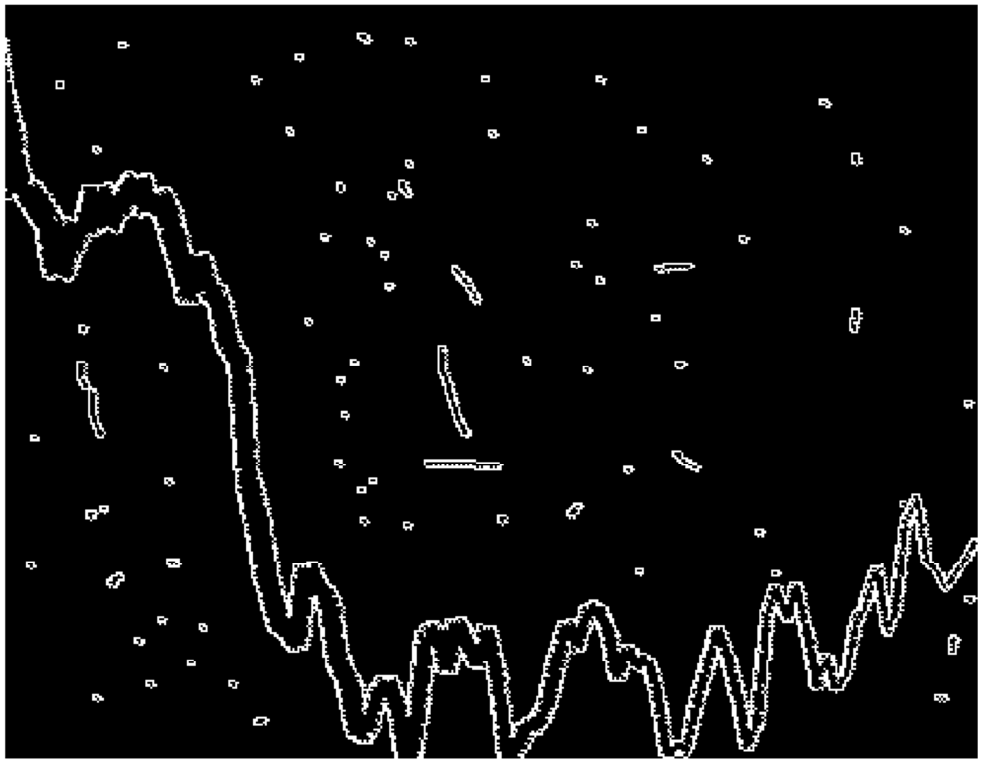

Group3-uneven illumination

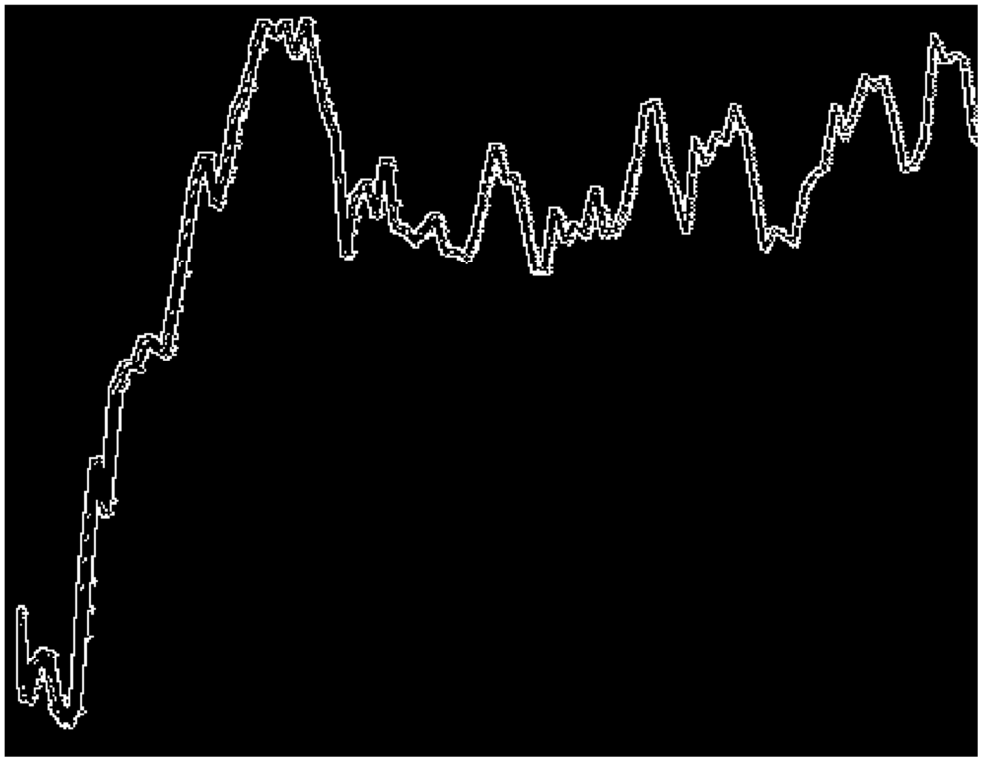

Large crack-disk

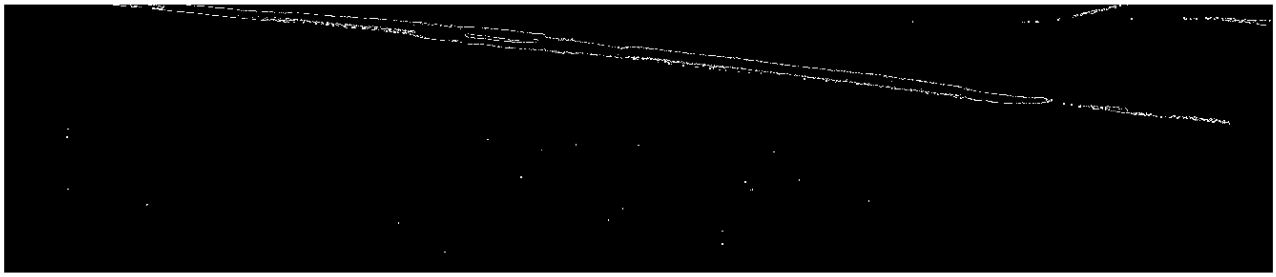

Crazing cracks

Stress cracks

Crazing cracks with background noises and boundary box